

Article

Excited State Hydroxide Ion Release From a Series of Acridinol Photobases

Yun Xie, Stefan Ilic, Sanja Skaro, Veselin Maslak, and Ksenija D. Glusac

J. Phys. Chem. A, **Just Accepted Manuscript** • DOI: 10.1021/acs.jpca.6b10980 • Publication Date (Web): 19 Dec 2016

Downloaded from <http://pubs.acs.org> on December 24, 2016

Just Accepted

“Just Accepted” manuscripts have been peer-reviewed and accepted for publication. They are posted online prior to technical editing, formatting for publication and author proofing. The American Chemical Society provides “Just Accepted” as a free service to the research community to expedite the dissemination of scientific material as soon as possible after acceptance. “Just Accepted” manuscripts appear in full in PDF format accompanied by an HTML abstract. “Just Accepted” manuscripts have been fully peer reviewed, but should not be considered the official version of record. They are accessible to all readers and citable by the Digital Object Identifier (DOI®). “Just Accepted” is an optional service offered to authors. Therefore, the “Just Accepted” Web site may not include all articles that will be published in the journal. After a manuscript is technically edited and formatted, it will be removed from the “Just Accepted” Web site and published as an ASAP article. Note that technical editing may introduce minor changes to the manuscript text and/or graphics which could affect content, and all legal disclaimers and ethical guidelines that apply to the journal pertain. ACS cannot be held responsible for errors or consequences arising from the use of information contained in these “Just Accepted” manuscripts.

1
2
3
4
5
6
7
8
9
10
11
12
13
14
15
16
17
18
19
20
21
22
23
24
25
26
27
28
29
30
31
32
33
34
35
36
37
38
39
40
41
42
43
44
45
46
47
48
49
50
51
52
53
54
55
56
57
58
59
60

Excited State Hydroxide Ion Release From a Series of Acridinol Photobases

Yun Xie,^{1†} Stefan Ilic,[†] Sanja Skaro,[‡] Veselin Maslak,[‡] Ksenija D. Glusac^{†}*

[†]Department of Chemistry, Center for Photochemical Sciences, Bowling Green State University,
Bowling Green, Ohio 43403, United States

[‡]Faculty of Chemistry, University of Belgrade, Studentski Trg 12-16, Belgrade 11000, Serbia

1
2
3 ABSTRACT. The excited-state heterolysis of acridinol-based derivatives leads to the release of
4 the OH^- ion and the formation of the corresponding acridinium cations. To evaluate the
5 parameters that control the reaction barriers, the kinetics of excited-state OH^- release from a
6 series of acridinol photobases were studied using transient absorption spectroscopy. The rate
7 constants were obtained in three solvents (methanol, butanol and isobutanol), and the data were
8 modeled using Marcus theory. The intrinsic reorganization energies obtained from these fits
9 were found to correlate well with the solvent reorganization energies calculated using dielectric
10 continuum model, suggesting that the excited-state OH^- release occurs along the solvent reaction
11 coordinate. Furthermore, the ability of acridinol photobases to photo-initiate chemical reactions
12 was demonstrated using the Michael reaction between dimethylmalonate and nitrostyrene.
13
14
15
16
17
18
19
20
21
22
23
24
25
26
27
28
29
30

31 INTRODUCTION

32
33
34 Photoacids are a group of molecules, usually containing the aromatic alcohol motif, whose
35 acidity significantly increases upon electronic excitation (up to 32 pK_a units).¹⁻³ The excitation of
36 photoacids in the presence of appropriate base acceptors enables mechanistic studies of fast
37 proton transfer (PT) reactions in solution using time-resolved laser techniques.⁴⁻⁹ These
38 experimental results provided a valuable platform to test and improve current theoretical models
39 for PT. For example, Nibbering discovered the transient signature of the solvated proton in the
40 mid-IR range during the PT between the pyranine photoacid and the acetate base, which offered
41 evidence of a solvent-mediated PT.⁷ Such solvent-mediated mechanism is not modeled in the
42 traditional Eigen-Weller theory for PT, which prompted Siwick and Bakker to develop an
43 improved model for PT that included a distribution of reactive acid-base species separated by a
44
45
46
47
48
49
50
51
52
53
54
55
56
57
58
59
60

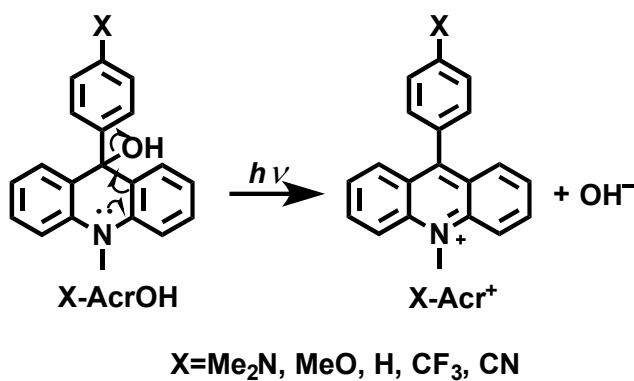
1
2
3 varying number of solvent molecules.⁸ In addition to these basic studies of PT mechanism, the
4
5 photoacids have also been applied to: (i) generate and characterize short-lived intermediates,
6
7 such as H₂CO₃;¹⁰ (ii) probe the microenvironment of the biological systems (protein pockets and
8
9 cells)¹¹⁻¹⁷ and other confined media (reverse micelles, cyclodextrins and nafion membranes);¹⁸⁻²⁰
10
11 (iii) study the protein folding kinetics using the pH jump technique.²¹⁻²²
12
13
14

15 In analogy to the photoacids described above, the photobases are defined here as compounds
16
17 that release hydroxide ion (OH⁻) upon excitation. Several types of photobases were identified in
18
19 the '80s and were composed of triarylmethanol, xanthenol, fluorenol and other molecular
20
21 frameworks.²³⁻²⁴ These early studies treated photobases as suitable sources of short-lived
22
23 carbocations, whose reactivity with various nucleophiles was studied using time-resolved
24
25 nanosecond laser spectroscopy.²⁵⁻²⁶ More recently, the pseudobase derivatives of aryltropylium
26
27 and acridinium ions have been investigated as a new class of photo-switches.²⁷⁻²⁹ The kinetics of
28
29 OH⁻ release were not addressed in these studies, likely due to the insufficient time resolution of
30
31 the nanosecond transient absorption instrument used. Nowadays, the availability of ultrafast
32
33 lasers allows chemists to capture the kinetics of OH⁻ release and investigate the mechanism of
34
35 OH⁻ transport in various media, which will likely contribute to our understanding of OH⁻
36
37 solvation and diffusion. For example, recent findings have challenged the traditional view of
38
39 OH⁻ solvation as [OH (H₂O)₃]⁻ species, “mirror image” of proton solvation), and proposed a
40
41 “hypercoordinated” configuration [OH(H₂O)₄]⁻, which seems to agree with the experimental
42
43 evidence.³⁰⁻³¹ With the unique light-triggered OH⁻ release, photobases will likely serve as an
44
45 excellent probe for time-resolved studies of OH⁻ solvation. Furthermore, photobases have
46
47 already been utilized to achieve spatiotemporal control in biologically relevant systems, to
48
49 trigger DNA/RNA conformational changes and drug delivery.³²⁻³⁴
50
51
52
53
54
55
56
57
58
59
60

1
2
3 We previously studied the kinetics of OH⁻ release from an acridinol photobase using
4 femtosecond pump-probe spectroscopy,³⁵ and found that the heterolysis is fast (108 ps lifetime)
5 in protic solvents (such as methanol), while no heterolysis occurs in aprotic solvent (such as
6 acetonitrile). This solvent-dependent OH⁻ release is quite similar to the previous studies of
7 excited-state PT,³ and is likely due to increased reactivity of the hydrogen-bonded complex
8 between the photoacid or the photobase with the accepting solvent molecules. To gain a more
9 quantitative comparison of the kinetics of H⁺/OH⁻ release, the intrinsic barrier for OH⁻ release
10 from a xanthenol photobase was evaluated in a series of solvent mixtures.³⁶ Using the Marcus
11 model, the intrinsic barrier was found to be $\Delta G_0^\ddagger \sim 10$ kcal/mol, which is significantly higher than
12 the barriers found previously for the PT ($\Delta G_0^\ddagger \sim 1-2$ kcal/mol).^{3, 37} Such differences in the
13 photoreactivity of photoacids and photobases could be due to differences in solvation of released
14 ions. Alternatively, the lower reactivity of OH⁻ release could be due to high reorganization
15 energy of the cation formed, or due to less efficient OH⁻ release relative to H⁺.³⁶

16
17
18
19
20
21
22
23
24
25
26
27
28
29
30
31
32
33
34 In this study, the role of the solvent reorganization on rates of excited-state OH⁻ release was
35 evaluated using a series of acridinol photobases (Scheme 1). Specifically, the thermodynamics
36 (ΔG) and kinetics (k) of the OH⁻ release were studied using steady-state and time-resolved
37 UV/VIS absorption spectroscopy. The experimental values were modeled using Marcus theory to
38 evaluate the intrinsic barrier ΔG_0^\ddagger for the OH⁻ release. The intrinsic reorganization energies
39 obtained from the Marcus fits were found to correlate very well with the solvent reorganization
40 energies predicted by a dielectric continuum model. These results indicate that the OH⁻ release
41 occurs along the solvent reaction coordinate and that the barrier height is controlled by the
42 solvent response to the formed charges.
43
44
45
46
47
48
49
50
51
52
53
54
55
56
57
58
59
60

1
2
3 This manuscript also reports that the acridinol photobases can be utilized to drive chemical
4 reactions. Previous approaches to photobase-driven reactions have mostly relied on bases
5 protected with photo-labile precursors.³⁸⁻⁴⁰ While these methods provide efficient base
6 generation, the process is irreversible. More recently, the reversibility was achieved using *cis-*
7 *trans* photoisomerization as a way to control the basicity of the photoactive molecule.⁴¹⁻⁴² Here,
8 we show that the irradiation of acridinol photobase can be utilized to drive a Michael addition
9 reaction. In specific, the reaction between dimethylmalonate and nitrostyrene was triggered using
10 AcrOMe photobase, which releases the methoxide ion upon excitation. The methoxide ion acts
11 as a base that deprotonates dimethylmalonate and initiates the addition to nitrostyrene. The
12 results of this study show that acridinol photobases can promote the base-catalyzed reactions,
13 which is expected to be useful in applications that require spatial or temporal control of the
14 chemical reactivity.



45 **Scheme 1.** The photochemical OH⁻ release from model 9-substituted acridinols.

46 47 48 49 50 51 EXPERIMENTAL SECTION

52
53 Syntheses. All chemicals were purchased from commercial suppliers and used without further
54 purification. ¹H and ¹³C NMR spectra were recorded on a Bruker Avance III 500 MHz system.

1
2
3
4
5
6
7
8
9
10
11
12
13
14
15
16
17
18
19
20
21
22
23
24
25
26
27
28
29
30
31
32
33
34
35
36
37
38
39
40
41
42
43
44
45
46
47
48
49
50
51
52
53
54
55
56
57
58
59
60

Electron impact ionization (EI) and MALDI mass spectra were measured on a Shimadzu QP5050A and a Bruker Daltonics Omnicflex mass spectrometer. 10-Methyl-9-phenylacridinium perchlorate (Acr^+) was purchased from TCI America. Aryl-bromides (4-bromoanisole, 4-bromobenzonitrile and 4-bromobenzotrifluoride) were purchased from Sigma. AcrOMe was synthesized according to already reported procedure.³⁵

10-methyl-9-phenyl-9,10-dihydroacridin-9-ol (AcrOH): AcrOH was synthesized according to the literature.³⁵ A 1 M solution of NaHCO_3 (100 ml) was added to 10-methyl-9-phenylacridinium perchlorate (Acr^+ , 225 mg, 0.6 mmol). Acetonitrile (~25 mL) was added to dissolve Acr^+ completely and the pH was then increased to 13 by addition of 30% aqueous NaOH. Conversion was monitored using UV/Vis by observing the disappearance of the absorption at 427 nm. When all Acr^+ converted to AcrOH, the reaction mixture was stirred for 15 min in the dark. Acetonitrile was removed in vacuo and water solution was extracted with dichloromethane (3x100 mL). Organic layers were combined, dried over anhydrous calcium chloride and solvent evaporated. Cyclohexane was added to the residue causing the precipitation of unreacted Acr^+ . Filtrate was collected and evaporated to give 95 mg of pure AcrOH (54%). MS-MALDI: m/z 287 [M^+ for $\text{C}_{20}\text{H}_{17}\text{NO}$], $^1\text{H-NMR}$ (CD_3CN , 500 MHz): δ 7.58 (d, 2H, $J = 7.7$ Hz), 7.35-7.31 (m, 2H), 7.22 (d, 4H, $J = 4.3$ Hz), 7.16-7.14 (m, 1H), 7.12 (d, 2H, $J = 8.2$ Hz), 7.01 (t, 2H, $J = 7.5$ Hz), 4.21 (br s, 1H), 3.49 (s, 3H). $^{13}\text{C-NMR}$ (CD_3CN , 125 MHz): δ 148.4, 140.0, 129.6, 128.1, 127.8, 126.7, 126.6, 125.6, 120.3, 112.4, 72.4, 32.7.

9-(4-(dimethylamino)phenyl)-10-methylacridin-10-ium perchlorate ($\text{Me}_2\text{N-Acr}^+$): $\text{Me}_2\text{N-Acr}^+$ was synthesized according to the literature under modified conditions.⁴³ Under nitrogen, 10-methyl-9(10H)-acridone (1 g, 4.8 mmol), *N,N*-dimethylaniline (1.36 mL, 10.7 mmol, 2.3 eq) and phosphoryl chloride (2.43 mL, 26.1 mmol, 5.4 eq) were mixed and left to stir for 2 hours at 90

1
2
3 °C. Concentrated aqueous sodium hydroxide solution was added carefully to quench the reaction.
4
5
6 The reaction mixture was then extracted with dichloromethane, organic layers were combined,
7
8 dried over anhydrous sodium sulfate and solvent evaporated under reduced vacuum. The oily
9
10 residue was dissolved in minimal volume of acetonitrile and perchloric acid was added until a
11
12 green-yellowish color. Protonated $\text{Me}_2\text{NH}^+\text{-Acr}^+$ dication was then extracted with
13
14 dichloromethane and solvent was evaporated. Upon addition of water to the green-yellow solid,
15
16 color changed to deep blue-purple. Target compound was extracted with dichloromethane, dried
17
18 over anhydrous sodium sulfate and solvent was evaporated. The crude solid product was
19
20 recrystallized from acetonitrile/ether mixture. Formed precipitate was filtered and washed with
21
22 copious amount of ether to yield 1.78 g of deep blue-purple solid (90%). $^1\text{H-NMR}$ (CD_3CN , 500
23
24 MHz): δ 8.54 (d, 2H, $J = 9.2$ Hz), 8.35 (dd, 1H, $J_1 = 6.8$ Hz, $J_2 = 1.5$ Hz), 8.33 (dd, 1H, $J_1 = 6.8$
25
26 Hz, $J_2 = 1.5$ Hz), 8.24 (dd, 2H, $J_1 = 6.8$ Hz, $J_2 = 0.8$ Hz), 7.85 (dd, 1H, $J_1 = 6.8$ Hz, $J_2 = 0.8$ Hz),
27
28 7.84 (dd, 1H, $J_1 = 6.8$ Hz, $J_2 = 0.8$ Hz), 7.48-7.45 (m, 2H), 7.13 (d, 2H, $J = 7.9$ Hz), 4.75 (s, 3H),
29
30 3.16 (s, 6H). $^{13}\text{C-NMR}$ (CD_3CN , 125 MHz): δ 162.9, 151.9, 141.7, 138.6, 132.7, 131.0, 127.2,
31
32 126.1, 119.6, 118.6, 111.7, 40.2, 39.0.
33
34
35
36
37
38

39 *9-(4-(dimethylamino)phenyl)-10-methyl-4a,9,9a,10-tetrahydroacridin-9-ol* ($\text{Me}_2\text{N-AcrOH}$):
40
41 $\text{Me}_2\text{N-Acr}^+$ (200 mg, 0.5 mmol) was dissolved in 10 mL of acetonitrile and pH was increased to
42
43 13 by addition of 5 M aqueous NaOH solution. The resulting solution was stirred for 2 h and
44
45 then extracted with dichloromethane. Organic layers were combined, dried over anhydrous
46
47 sodium sulfate and solvent evaporated. Crude product was dissolved in hexane/benzene mixture
48
49 (2:1) to precipitate the remaining starting material. Filtrate was collected and evaporated to give
50
51 85 mg of pure product (60%). MS-EI: m/z 312 [M^+ calculated for $\text{C}_{21}\text{H}_{16}\text{N}_2\text{O}$], $^1\text{H-NMR}$
52
53 (CD_3CN , 500 MHz): δ 7.65 (dd, 2H, $J_1 = 7.7$ Hz, $J_2 = 1.5$ Hz), 7.34-7.31 (m, 2H), 7.10 (d, 2H, J
54
55
56
57
58
59
60

1
2
3 = 8.3 Hz), 7.03 (td, 2H, $J_1 = 7.7$ Hz, $J_2 = 1.1$ Hz), 6.98-6.94 (m, 2H), 4.02 (br s, 1H), 3.46 (s,
4
5 3H), 2.84 (s, 6H). ^{13}C -NMR (CDCl_3 , 125 MHz): δ 162.8, 151.9, 141.6, 138.6, 132.7, 131.0,
6
7 127.2, 126.1, 119.6, 118.6, 113.3, 111.7, 77.2, 40.2, 39.0.
8
9

10
11 *MeO-AcrOH*, *CN-AcrOH* and *CF₃-AcrOH* were synthesized according to the following
12 procedure: To a solution of corresponding aryl-bromide (2 mmol) in dry THF (6 mL), 2.5 M
13 hexane solution of *n*-butyllithium (0.96 mL, 2.4 mmol) was added dropwise at -78 °C under
14 argon and stirred for 30 min. A suspension of 10-methyl-9(10H)-acridone (0.33 g, 1.6 mmol) in
15 dry THF (14 mL) was then added and the resulting solution stirred for 12 h at room temperature.
16 The reaction was quenched by addition of 20 mL of saturated aqueous ammonium chloride
17 solution and extracted with dichloromethane (3x10 mL). Organic fractions were combined, dried
18 over anhydrous magnesium sulfate and solvent evaporated. Crude product was dissolved in
19 hexane/benzene mixture (2:1) causing the precipitation of the remaining starting material. The
20 filtrate containing desired product was collected and solvent removed in vacuo to give desired
21 acridinol.
22
23
24
25
26
27
28
29
30
31
32
33
34
35

36
37 *9-(4-methoxyphenyl)-10-methyl-9,10-dihydroacridin-9-ol (MeO-AcrOH)*: Using the procedure
38 described above, 0.25 g of pure product (49%) was obtained. MS-EI: m/z 317 [M^+ calculated for
39 $\text{C}_{21}\text{H}_{19}\text{NO}_2$], ^1H -NMR (CD_3CN , 500 MHz): δ 7.62 (dd, 2H, $J_1 = 7.7$ Hz, $J_2 = 1.5$ Hz), 7.34 (dd,
40 1H, $J_1 = 7.0$ Hz, $J_2 = 1.4$ Hz), 7.33 (dd, 1H, $J_1 = 7.0$ Hz, $J_2 = 1.4$ Hz), 7.12 (d, 2H, $J = 7.7$ Hz),
41 7.10-7.07 (m, 2H), 7.03 (td, 2H, $J_1 = 7.7$ Hz, $J_2 = 1.1$ Hz), 6.77-6.74 (m, 2H), 4.11 (s, 1H), 3.72
42 (s, 3H), 3.48 (s, 3H). ^{13}C -NMR (CD_3CN , 125 MHz): δ 158.3, 140.5, 140.1, 129.8, 128.0, 126.9,
43 126.4, 120.2, 113.0, 112.3, 72.0, 54.8, 32.9.
44
45
46
47
48
49
50
51
52

53
54 *4-(9-hydroxy-10-methyl-9,10-dihydroacridin-9-yl)benzotrile (CN-AcrOH)*: Using the given
55 procedure, 0.31 g of pure product (48%) was obtained. MS-EI: m/z 312 [M^+ calculated for
56
57
58
59
60

1
2
3 $C_{21}H_{16}N_2O$], 1H -NMR (CD_3CN , 500 MHz): δ 7.56-7.53 (m, 2H), 7.51 (dd, 2H, $J_1 = 7.7$ Hz, $J_2 =$
4 1.4 Hz), 7.39 (d, 2H, $J = 8.3$ Hz), 7.35-7.30 (m, 2H), 7.12 (d, 2H, $J = 8.3$ Hz), 6.98 (t, 2H, $J =$
5 7.5 Hz), 4.49 (s, 1H), 3.48 (s, 3H). ^{13}C -NMR (CD_3CN , 125 MHz): δ 154.5, 140.7, 132.8, 129.5,
6 127.6, 127.2, 121.4, 113.6, 110.9, 72.9, 33.9.
7
8
9

10
11
12 10-methyl-9-(4-(trifluoromethyl)phenyl)-9,10-dihydroacridin-9-ol (CF_3 -Acr-OH): Using the
13 given procedure, 0.39 g of pure product (55%) was obtained. MS-EI: m/z 355 [M^+ calculated for
14 $C_{21}H_{16}NF_3$], 1H -NMR (CD_3CN , 500 MHz): δ 7.57-7.53 (m, 4H), 7.45 (d, 2H, $J = 8.6$ Hz), 7.36
15 (ddd, 2H, $J_1 = 8.7$ Hz, $J_2 = 7.2$ Hz, $J_3 = 1.6$ Hz), 7.16 (d, 2H, $J = 8.3$ Hz), 7.02 (td, 2H, $J_1 = 7.8$
16 Hz, $J_2 = 1.6$ Hz), 4.40 (s, 1H), 3.52 (s, 3H). ^{13}C -NMR (CD_3CN , 125 MHz): δ 153.7, 140.7,
17 129.6, 129.4, 128.9 (q, $J_{CF} = 32$ Hz), 127.7, 127.1, 125.7 (q, $J_{CF} = 3.8$ Hz), 121.2, 113.5, 73.0,
18 33.8.
19
20
21
22
23
24
25
26
27
28

29 Equilibrium constant determination. UV/Vis absorption spectra were recorded on Varian Cary
30 50 Bio spectrometer in a 1 cm quartz cell from 200 nm to 800 nm. The sample concentration was
31 controlled so that the absorption maximum was around 1. Fluorescence measurements were
32 performed on a single photon counting spectrofluorimeter from Edinburgh Analytical
33 Instruments (FL/FS 920) in a 1 cm quartz cell. The excitation wavelengths and the emission
34 spectral windows were chosen according to each sample. The concentration of the samples was
35 diluted 100 times from absorption measurements. The ground-state pK_{OH} values were
36 determined as described previously with a slight modification.³⁵ The equilibrium constant K_{OH}
37 was determined by titrating the solutions of acridinium cations ($X-Acr^+$) with a solution of
38 sodium hydroxide with known concentration (it was assumed that NaOH fully dissociates in the
39 solvent) and the concentrations of $X-Acr^+$ and $X-AcrOH$ were determined using UV/Vis
40
41
42
43
44
45
46
47
48
49
50
51
52
53
54
55
56
57
58
59
60

1
2
3 absorption spectroscopy. The K_{OH} was calculated from the solution in which 50% of Acr^+ is
4
5 converted to $AcrOH$, as:
6
7

$$8 \quad K_{OH} = [OH^-] = c_{NaOH} - \frac{c_{X-Acr^+}}{2}$$

9
10 Femtosecond Transient Absorption Experiments. The 800 nm laser pulses were produced at a
11
12 1 kHz repetition rate by a mode-locked Ti:sapphire laser and regenerative amplifier (Hurricane,
13
14 Spectra-Physics). The output from the Hurricane was split into pump (85%) and probe (10%)
15
16 beams. The pump beam was sent into an optical parametric amplifier (OPA-400, Spectra
17
18 Physics) to obtain the desired excitation wavelength. The energy of the pump beam was <300
19
20 nJ/pulse. The probe beam was focused into a two-dimensional translated 4 mm CaF_2 crystal for
21
22 white light generation between 350 and 800 nm. The flow cell (Starna Cell Inc. 45-Q-2, 0.9 mL
23
24 volume with 2 mm pathlength), pumped by a Variable Flow Mini-Pump (Control Company),
25
26 was used to prevent photo-degradation of the sample. After passing through the cell at the magic-
27
28 angle geometry, the continuum was coupled into an optical fiber and input into a CCD
29
30 spectrograph (Ocean Optics, S2000). The data acquisition was achieved using in-house
31
32 LabVIEW (National Instruments) software routines. The group velocity dispersion of the
33
34 probing pulse was determined using nonresonant optical Kerr effect (OKE) measurements.
35
36 Sample solutions were prepared at a concentration needed to have absorbance of 1.0 at the
37
38 excitation wavelength.
39
40
41
42
43
44
45

46 Photo-Michael addition. The model Michael addition was performed by preparing a solution of
47
48 10.5 mg of *trans*- β -nitrostyrene (0.0706 mmol, 1 eq), 8.1 μ L of dimethylmalonate (0.0706 mmol,
49
50 1 eq) and 21.3 mg $AcrOMe$ (0.0706 mmol, 1 eq) in 0.5 mL methanol. The protocol involved
51
52 either thermal or photochemical treatment. In the thermal treatment, the reaction mixture was
53
54 stirred for 24 h at 65 $^{\circ}C$. In the photochemical treatment, the reaction mixture was irradiated (125
55
56
57
58
59
60

1
2
3 W medium pressure mercury lamp) for 3 min and then stirred for 24 h at 65 °C. After each
4
5 treatment, the reaction was quenched by addition of water and the reaction mixture was extracted
6
7 with dichloromethane. Organic layers were combined, dried over anhydrous sodium sulfate and
8
9 solvent evaporated. Oily crude product was purified with dry-flash chromatography
10
11 (hexane/ethyl acetate = 8/2) to yield the oily product (thermal treatment gave 8.3 mg of the
12
13 product or 38%, while the photochemical treatment gave 13 mg of the product or 60%). ¹H-
14
15 NMR (CDCl₃, 500 MHz): δ 7.34-7.28 (m, 3H), 7.24-7.22 (m, 2H), 4.95-4.86 (m, 2H), 4.24 (td,
16
17 1H $J_1 = 9.0$ Hz, $J_2 = 5.1$ Hz), 3.87 (d, 1H, $J = 9.0$ Hz), 3.76 (s, 3H), 3.56 (s, 3H). ¹³C-NMR
18
19 (CDCl₃, 125 MHz): δ 168.0, 167.5, 136.4, 129.3, 128.6, 128.1, 77.6, 55.0, 53.2, 53.0, 43.2.
20
21
22
23
24
25
26

27 RESULTS AND DISCUSSION

28
29 Model compounds: The driving force for the excited-state OH⁻ transfer was tuned by
30
31 preparing a series of model acridinol compounds with varying substituents on the phenyl ring
32
33 (Scheme 1). These acridinol derivatives were readily synthesized using a reaction between N-
34
35 methyl-acridone and the corresponding aryl-lithium reagent, as described in the Experimental
36
37 Section. The absorption and emission spectra of the model acridinol photobases X-AcrOH and
38
39 their corresponding acridinium salts X-Acr⁺ are shown in Figure 1. In general, the
40
41 absorption/emission maxima of all acridinol X-AcrOH derivatives appear at shorter wavelengths
42
43 than the bands of the corresponding X-Acr⁺ cations, which is consistent with the increased
44
45 conjugation of the X-Acr⁺ cations.
46
47
48
49

50
51 The red-shifts in the absorption/emission bands were observed for the model compounds that
52
53 can form charge-transfer excited states. For example, the emission bands of X-AcrOH
54
55 derivatives with electron-withdrawing groups (478 nm for CN-AcrOH and 412 nm for CF₃-
56
57
58
59
60

1
2
3
4
5
6
7
8
9
10
11
12
13
14
15
16
17
18
19
20
21
22
23
24
25
26
27
28
29
30
31
32
33
34
35
36
37
38
39
40
41
42
43
44
45
46
47
48
49
50
51
52
53
54
55
56
57
58
59
60

AcrOH) appear at higher wavelengths than the emission bands of other acridinols (~350 nm), which is likely due to the formation of charge transfer excited state, in which the electron density migrates from the acridinol moiety to the substituted phenyl ring. Similarly, the emission band of Me₂N-Acr⁺ (680 nm) is red-shifted relative to emission bands of other acridinium cations (~510 nm), likely due to the formation of a charge transfer state in which the electron density moves from the substituted phenyl ring to the acridinium moiety. Similar charge-transfer states were reported in other acridinium salts.⁴⁴

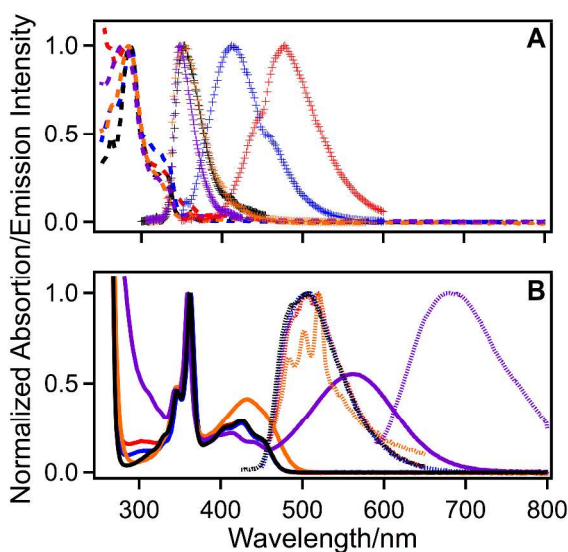
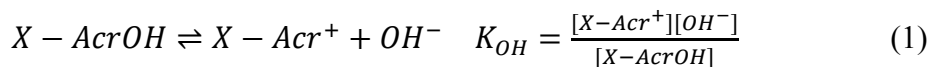


Figure 1. Absorption and emission spectra of A) X-AcrOH and B) X-Acr⁺. All of the spectra were collected in acetonitrile at room temperature, except for Me₂N-Acr⁺, whose emission spectrum was collected in 2-methyltetrahydrofuran at 77 K). AcrOH/Acr⁺ (black), Me₂N-AcrOH/Me₂N-Acr⁺ (purple), MeO-AcrOH/MeO-Acr⁺ (orange), CF₃-AcrOH/ CF₃-Acr⁺ (blue), CN-AcrOH/CN-Acr⁺ (red); X-AcrOH absorption (dash line), X-AcrOH emission (+ marker), X-Acr⁺ absorption (solid line), X-Acr⁺ emission (dotted line).

THERMODYNAMICS

The thermodynamic driving force for the excited-state OH⁻ release from model acridinol derivatives was evaluated in four different solvents (water, methanol, butanol and isobutanol).

First, the ground-state pK_{OH} and ΔG_{OH} values for the reaction:



were obtained using pH-dependent UV/Vis absorption spectroscopy. The results indicate that the OH⁻ release from acridinol models in their ground state is thermodynamically unfavorable in all solvents (Table 1). The thermodynamic parameters for CF₃-AcrOH and CN-AcrOH in *n*-BuOH and *i*-BuOH were not obtained, because the excited-state OH⁻ release was not observed for these X-AcrOH/solvent systems. Across the acridinol series, the driving force increases with the electron-donating character of the substituent (for example, the lowest ΔG value was obtained for Me₂N-AcrOH). This result is consistent with the fact that electron-donating groups stabilize the X-Acr⁺ cations formed upon OH⁻ release by positive charge delocalization. Similarly, previous studies have shown that the driving force for OH⁻ release in other pseudobases correlates well with factors that tend to stabilize the corresponding cations.⁴⁵⁻⁴⁷ For example, the driving force for OH⁻ release from xanthenol (XanOH) in water is $\Delta G=18.8$ kcal/mol,³⁶ which is significantly higher than for acridinol AcrOH ($\Delta G=3.9$ kcal/mol), reflecting the higher aromatic character of acridinium cation Acr⁺ relative to Xan⁺. The solvent effects on the driving force is as expected: the high polarity solvents (water) are better at stabilizing the ions formed upon heterolysis, which lowers the ΔG values for OH⁻ release. Similar solvent polarity effects were observed in the photoacids.⁴⁸

Table 1. Ground-state pK_{OH} and ΔG_{OH} values for model X-AcrOH acridinols in different solvents.

X	H ₂ O		MeOH		<i>n</i> -BuOH ^a		<i>i</i> -BuOH ^a	
	pK_{OH}	ΔG_{OH}	pK_{OH}	ΔG_{OH}	pK_{OH}	ΔG_{OH}	pK_{OH}	ΔG_{OH}
Me ₂ N	2.3	3.2	4.0	5.5	5.1	7.0	4.4	6.1
MeO	2.7	3.7	4.5	6.1	4.9	6.8	5.0	6.8
H	2.8	3.9	4.7	6.4	5.2	7.2	6.1	8.3
CF ₃	3.2	4.4	5.6	7.7	-	-	-	-
CN	3.3	4.5	5.8	8.0	-	-	-	-

^aThe calculations assume that NaOH is fully dissociates in *n*-BuOH and *i*-BuOH.

The ground-state pK_a values were then used to derive the excited-state thermodynamics using the Förster cycle,³⁵ as follows:

$$\Delta G_{OH}^* = hv_{X-AcrOH} - \Delta G_{OH} - hv_{X-Acr^+} \quad (2)$$

For this purpose, the frequencies for 0–0 transitions of X-AcrOH and X-Acr⁺ were derived from the emission spectra of the model compounds (Figure 1). The resulting ΔG_{OH}^* values (Table 2) show that the driving force for OH⁻ release considerably increases upon excitation. For example, the driving force for Me₂N-AcrOH in methanol changes from 5.5 kcal/mol in the ground state to -35.7 kcal/mol in the excited state. In other acridinols, similar but less drastic changes in ΔG values occur, and the excited-state OH⁻ release is thermodynamically favored in all compounds except for CN-AcrOH.

Table 2. Excited-state pK_{OH}^* and ΔG_{OH}^* values for model X-AcrOH acridinols in different solvents.

X	H ₂ O		MeOH		<i>n</i> -BuOH		<i>i</i> -BuOH	
	pK_{OH}^*	ΔG_{OH}^*	pK_{OH}^*	ΔG_{OH}^*	pK_{OH}^*	ΔG_{OH}^*	pK_{OH}^*	ΔG_{OH}^*
Me ₂ N	-27.2	-37.3	-25.5	-35.7	-25.1	-34.2	-25.8	-35.1
MeO	-16.1	-22.1	-14.4	-19.7	-13.9	-19.0	-13.8	-19.0
H	-15.0	-20.6	-13.2	-18.1	-12.7	-17.4	-11.8	-16.2
CF ₃	-6.4	-8.8	-3.9	-6.0	-	-	-	-
CN	0.7	1.0	3.3	4.4	-	-	-	-

The experimental pK_{OH} and pK_{OH}^* values correlate linearly with the Hammett σ coefficients⁴⁹ for the X-substituents (Figure 2), demonstrating that the simple free-energy relationship concept can be used efficiently to predict the driving force for the OH⁻ release. Similar linear relationship with a slope of opposite sign was observed for the photoacids,³⁴ indicating that the driving force for H⁺ or OH⁻ release is controlled by stabilization of charges formed upon the ion release (RO⁻ for photoacids and R⁺ for photobases). Interestingly, the slope ρ is significantly steeper for the excited-state pK_{OH}^* values ($\rho^*=14.8$ in water) than for the ground-state pK_{OH} values ($\rho=0.6$ in water). Thus, the electron-donating substituents in the X-position appear to stabilize more efficiently the positive charge of X-Acr⁺ in its S₁ state than in the S₀ state. Similar effects were observed in naphthol-based photoacids, where the substituent effects were found to correlate with the calculated charge densities of relevant atoms in their ground and excited states.³ It is likely that a similar effect holds for X-AcrOH photobases.

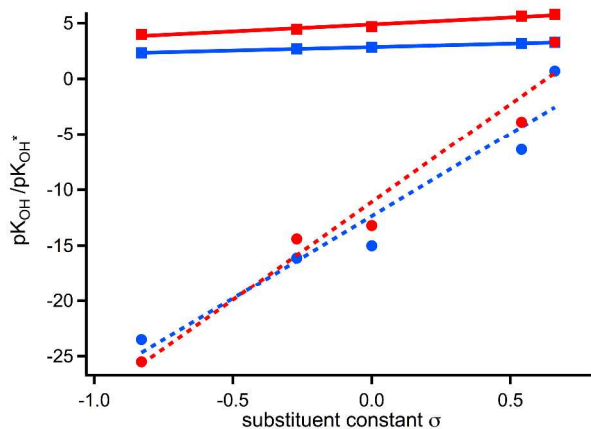


Figure 2. Hammett plots for ground (squares and solid lines) and excited-state (circles and dashed lines) OH^- release from X-AcrOH in water (blue) and methanol (red). The slopes are as follows: for ground states $\rho = 0.6$ in water and 1.2 in methanol; for excited-states $\rho^* = 14.8$ in water and 17.6 in methanol.

KINETICS

The rates of OH^- release from model acridinols were determined using pump-probe spectroscopy. The spectral changes in the visible range were consistent with the photochemical heterolysis of the C–O bond (Figure 3). For example, the transient absorption spectrum of the methanol solution of $\text{Me}_2\text{N-AcrOH}$ at early times (red trace, Figure 3A) was assigned to its S_1 state and exhibited broad features throughout the visible range with $\lambda_{\text{max}}=748$ nm. The S_1 signal decayed within few hundreds picoseconds and was accompanied with a concomitant growth of a new transient that absorbed at $\lambda_{\text{max}}=553$ nm. The absorption spectrum of this growing transient matched well to the spectrum of $\text{Me}_2\text{N-Acr}^+$ cation in the S_0 state (Figure 3A, dashed line), which is consistent with the excited state OH^- release from $\text{Me}_2\text{N-AcrOH}$. In a similar fashion, the conversion from excited MeO-AcrOH , AcrOH and $\text{CF}_3\text{-AcrOH}$ in methanol leads to the formation of the corresponding cations (Figures 3B-D). In the case of CN-AcrOH , the excited-state OH^- release was not observed, which is consistent with the unfavorable thermodynamics

($\Delta G^* = + 1.0$ kcal/mol, Table 2) and shows that the rates of the OH^- release correlate with the ΔG^* values calculated using simple Förster cycle.

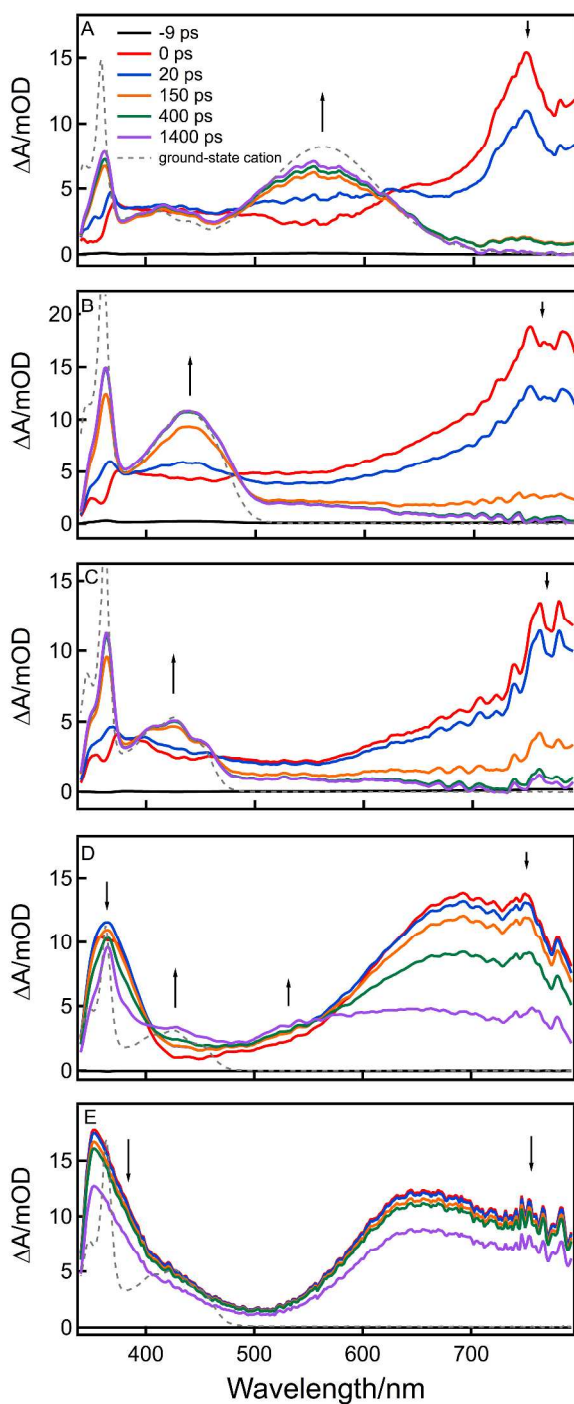


Figure 3. Femtosecond transient absorption spectra of X-AcrOH in MeOH at several time delays after the 310 nm excitation pulse: A) $\text{Me}_2\text{N-AcrOH}$; B) MeO-AcrOH ; C) AcrOH ; D) $\text{CF}_3\text{-AcrOH}$

1
2
3 AcrOH; E) CN-AcrOH. The dashed lines represent the ground-state absorption spectra for the
4
5
6 corresponding X-Acr⁺ cations.
7
8
9

10
11 Two similarities can be drawn between the photo-heterolysis observed in photoacids^{37, 50} and
12 the photobases studied here: (i) the rates of heterolysis correlate well with the driving force for
13 the adiabatic process (ΔG^*), as discussed in the previous paragraph; (ii) the excited-state
14 heterolysis occurs predominantly in protic solvents (such as alcohols). For example, MeO-
15 AcrOH undergoes efficient excited-state OH⁻ release in *n*-BuOH (Figure 4A), while S₁→T₁ ISC
16 occurs in acetonitrile (Figure 4B). Such dependence is suggestive of the important role that the
17 solvent reorganization energy plays in the H⁺ and OH⁻ release from organic alcohols.^{2, 48} One
18 notable difference exists between the excited state behavior of photoacids and photobases: the
19 PT generally occurs adiabatically, while the OH⁻ transfer occurs non-adiabatically in most
20 photobases. For example, the fluorescence spectra of photoacids in protic solvents generally
21 contain a variable degree of the red-shifted emission due to the conjugate base formed upon the
22 PT, confirming its adiabatic nature.⁵¹ On the other hand, the transient absorption spectra of
23 X-AcrOH derivatives (Figure 3 and ref. 35) show that X-Acr⁺ cations are formed in the ground
24 state, suggesting a non-adiabatic process. To the best of our knowledge, only two previous
25 reports showed adiabatic OH⁻ release from a xanthenol photobase,^{23, 52} but even in this case the
26 adiabatic process was a minor heterolysis channel, while most of the OH⁻ release occurred non-
27 adiabatically.
28
29
30
31
32
33
34
35
36
37
38
39
40
41
42
43
44
45
46
47
48
49
50
51
52
53
54
55
56
57
58
59
60

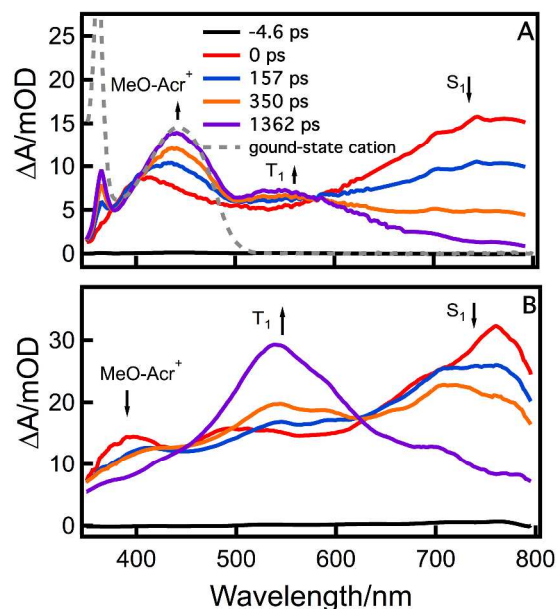


Figure 4. Femtosecond transient absorption data for MeO-AcrOH in A) *n*-BuOH and B) ACN.

The samples were excited at 310 nm.

The kinetics of S_1 states in all model X-AcrOH derivatives can be readily obtained by probing the red portion of the visible spectrum (for example $\lambda=750$ nm, Figure 5). The observed rate of S_1 decay increases along X-AcrOH series (Figure 5A), with faster decay occurring for electron-donating groups (such as $\text{Me}_2\text{N-AcrOH}$). The result is consistent with the ΔG^* values listed in Table 2: the photo-heterolysis rate increases as the process becomes more thermodynamically favorable. The solvent effects on the rate of OH^- release are shown in Figure 5B: the faster heterolysis is observed in higher polarity solvent (the solvent dielectric constants are as follows: $\epsilon_{\text{MeOH}}=33.0$, $\epsilon_{n\text{-BuOH}}=17.8$, $\epsilon_{i\text{-BuOH}}=17.9^{53}$). The solvent effects are consistent with increased stability of product ions by polar solvents, and this stabilization is reflected in the thermodynamic driving forces (Table 2). The polarities of *n*-BuOH and *i*-BuOH are similar, but

i-BuOH is bulkier. The observed rate does not change significantly in the two solvents, indicating that the solvent polarity plays the deciding role on the rate of OH⁻ release.

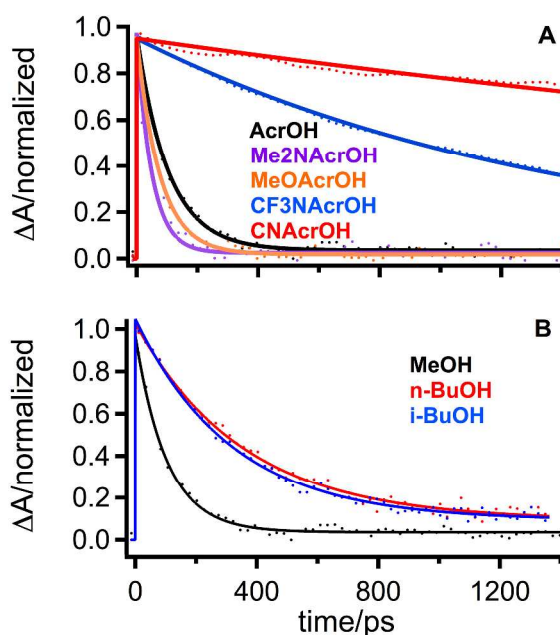


Figure 5. A) Normalized transient absorption traces ($\lambda_{\text{probe}}=750$ nm) for X-AcrOH solutions in MeOH ($\lambda_{\text{pump}}=310$ nm). Lifetime: Me₂N-AcrOH 53 ps; MeO-AcrOH 76 ps; AcrOH 108 ps; CF₃-AcrOH 1.4 ns; CN-AcrOH 6.3 ns; B) The kinetic trace for AcrOH ($\lambda_{\text{pump}}=310$ nm; $\lambda_{\text{probe}}=750$ nm) in MeOH (108 ps), *n*-BuOH (357 ps) and *i*-BuOH (319 ps).

In all model compounds, the 750 nm signal exhibited mono-exponential decay with rate constants k_{exp} (Table 3). As the rate of OH⁻ release slows down across the X-AcrOH series, the process starts to compete with the S₁→T₁ IC. Our earlier work on AcrOH³⁵ has shown that the excited-state OH⁻ release occurs only in protic solvents (methanol), while ISC dominates the excited-state deactivation in aprotic solvents (acetonitrile). Similar behavior in aprotic solvents was observed for most X-AcrOH derivatives (data not shown), which allowed the determination of ISC rates for each acridinol (k_{ISC}). The competition between heterolysis and ISC can be visualized in the case of CF₃-AcrOH (Figure 3D). In addition to the growth of CF₃-Acr⁺

absorption bands ($\lambda_{\text{ABS}}=425$ nm), additional absorption appears in the 500-600 nm and is assigned to the T_1 state of $\text{CF}_3\text{-AcrOH}$. Thus, the rates for OH^- release were obtained as follows:

$$k_{\text{OH}} = k_{\text{exp}} - k_{\text{ISC}} \quad (3)$$

The resulting k_{OH} values are listed in Table 3. The use of equation (3) assumes that the rate of ISC does not change significantly when going from acetonitrile to the alcohols studied here. Such assumption likely introduced an error in the estimated k_{OH} values, since previous reports indicate that some compounds exhibit relatively strong solvent effects on their ISC rates.⁵⁴⁻⁵⁵ However, since the triplet excited state absorption energy does not change significantly in different solvents (for example, triplet excited state of MeO-AcrOH absorbs at 550 nm in both ACN and $n\text{-BuOH}$, Figure 4), it is likely that the above assumption is justified.

Table 3. Experimental rate constants (k_{exp}) for the singlet excited state decays of X-AcrOH models and the derived rates for OH^- release (k_{OH}) determined as described in the text.

X	MeOH		$n\text{-BuOH}$		$i\text{-BuOH}$	
	$k_{\text{exp}}/10^9 \text{ s}^{-1}$	$k_{\text{OH}}/10^9 \text{ s}^{-1}$	$k_{\text{exp}}/10^9 \text{ s}^{-1}$	$k_{\text{OH}}/10^9 \text{ s}^{-1}$	$k_{\text{exp}}/10^9 \text{ s}^{-1}$	$k_{\text{OH}}/10^9 \text{ s}^{-1}$
Me_2N	0.2	0.2	3.7	3.0	4.3	3.6
MeO	0.1	0.1	3.4	2.4	3.8	2.9
H	9.3	9.3	3.1	2.4	3.1	2.4
CF_3	70.9	53.3	–	–	–	–
CN	15.9	-	–	–	–	–

The obtained k_{OH} values were used to construct their dependence on the thermodynamic driving force (Figure 6). To model the rate constant dependence on the thermodynamic driving

force, the well-known transition-state theory expression was used. It relates the rate constants with the corresponding energy barriers:

$$k = A \cdot e^{-\frac{\Delta G^\ddagger}{RT}} \quad (4)$$

where A is the pre-exponential factor and ΔG^\ddagger is the Gibbs free energy for the transition state. Two theoretical models were then used to correlate the dependence of ΔG^\ddagger on the thermodynamic driving force, ΔG^0 . One treatment utilized the Marcus model,⁵⁶⁻⁵⁹ which has been successfully applied to group transfers in which reaction rate is controlled by the response of the solvent to the charge redistribution. In this case, the reaction proceeds along the solvent reaction coordinate and the free energy correlation is:

$$\Delta G^\ddagger = \left(1 + \frac{\Delta G^0}{4 \cdot \Delta G_0^\ddagger}\right)^2 \cdot \Delta G_0^\ddagger \quad (5)$$

where ΔG_0^\ddagger is the activation energy for the symmetric group transfer ($\Delta G^0=0$). The second treatment utilized the bond-energy bond-order (BEBO) theory,⁶⁰⁻⁶² which models reactions that occur in a strong coupling regime, where the bond stretching and compression define the reaction coordinate. The BEBO model evaluates the energy of a reacting system at any point along the reaction coordinate using a linear combination of reactant and product energies, which are scaled by their bond order at a given point of the reaction coordinate. According to BEBO model, the free energy correlation is expressed as:

$$\Delta G^\ddagger = \frac{\Delta G^0}{2} + \Delta G_0^\ddagger + \frac{\Delta G_0^\ddagger}{\ln 2} \cdot \ln \left(\cosh \left(\frac{\Delta G^0 \cdot \ln 2}{2 \cdot \Delta G_0^\ddagger} \right) \right) \quad (6)$$

At lower driving forces, both Marcus and BEBO models predict similar rate dependence on the driving force, where the rate increases with increasing driving force. At large driving forces, however, the two models predict different behavior: while the Marcus model predicts a decrease in the rate at high driving forces (inverted region), the BEBO model predicts the rates to level off

at high driving forces (Figure 6). In the case of OH^- release from photobases, it is not known whether the rate-determining process involves predominantly the solvent reorganization or the reorganization of the molecular bonds; therefore the data were evaluated using both models.

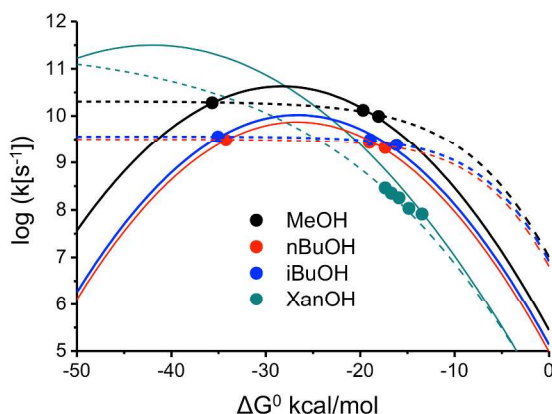


Figure 6. The dependence of k_{OH} values on thermodynamic driving forces for the excited-state OH^- release from model X-AcrOH derivatives. The fits were obtained using either Marcus (solid lines) or BEBO (dashed lines) model. The results of a previous study involving a xanthenol (XanOH) photobase³⁶ in acetonitrile/water mixtures are included for comparison.

Unfortunately, the limited range and number of experimental data points precluded us from evaluating whether Marcus or BEBO theory is better at modeling the excited-state OH^- release from our model compounds. However, it is interesting to note that the reorganization energies λ obtained using the Marcus model (Table 4) for AcrOH photobases in alcohol-based solvents match reasonably well with the expected solvent reorganization energies λ_s at the contact distance calculated using the dielectric continuum expression:⁶³⁻⁶⁴

$$\lambda_s = \frac{e^2}{4\pi\epsilon_0} \left(\frac{1}{2r_D} + \frac{1}{2r_A} - \frac{1}{r} \right) \left(\frac{1}{\epsilon_{op}} - \frac{1}{\epsilon_s} \right) \cdot N_A \quad (7)$$

where ϵ_{op} and ϵ_s are optical and static dielectric constants of the solvent, r_D and r_A are the donor and acceptor radii (we assumed that the radii are 3 Å each) and r is the distance between donor and acceptor. Based on these values, it appears that the excited state OH^- release from model acridinol photobases occurs along the reaction coordinate involving solvent responses and can be predicted well using the Marcus model.

Table 4. Summary of the parameters obtained from Marcus and BEBO analyses.

solvent	Marcus				BEBO	
	A	ΔG_0^\ddagger kcal/mol	λ^b kcal/mol	λ_s kcal/mol	A	ΔG_0^\ddagger kcal/mol
ACN/H ₂ O ^a	11.5	10.8	43.2	29.1-30.5	11.5	10.2
MeOH	10.6	7.1	28.3	29.8	10.3	4.5
<i>n</i> -BuOH	9.9	6.7	26.6	25.2	9.5	3.7
<i>i</i> -BuOH	10.0	6.7	26.6	25.3	9.6	3.6

a. For XanOH photobase, taken from ref. 36.

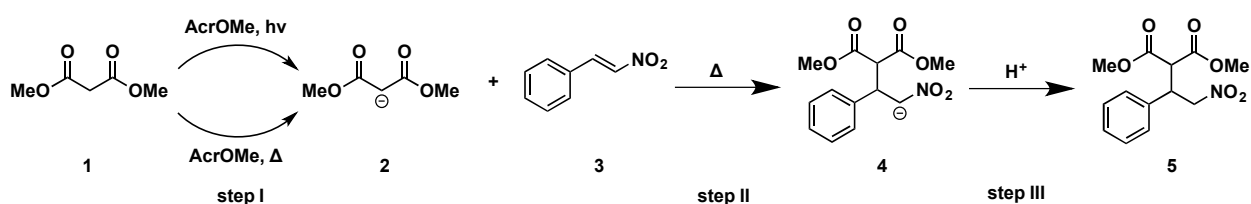
b. $\lambda = 4\Delta G_0^\ddagger$

The above results obtained in alcohol solvents are in contrast with the results reported in our previous study involving xanthenol (XanOH) photobase in acetonitrile/water mixtures.³⁶ The Marcus fit from this study provided a value for reorganization energy of $\lambda=43.2$ kcal/mol, which is significantly higher than the solvent reorganization energy of $\lambda_s=29.1-30.5$ kcal/mol calculated using the dielectric continuum model for acetonitrile and water (Table 4). Since the structures of XanOH and AcrOH photobases are quite similar, the differences in reorganization energies are likely due to solvents used. The dielectric continuum model is known to fail in predicting the

solvent reorganization energies in cases when there are specific reactant-solvent interactions.⁶⁵⁻⁶⁷ When such non-continuum factors are present, the experimentally observed rates are generally slower than those predicted by the continuum model, which is consistent with our results for XanOH in water/ACN mixtures.³⁶

PHOTO-MICHAEL ADDITION

The utility of photobases to drive chemical reaction has been reported previously, namely to drive Henry⁴¹ and thiol-Michael additions.⁶⁸⁻⁶⁹ In both of these examples, the photochemical event generates an amine, which serves as a base to drive the chemical reaction of interest. In a similar fashion, the acridine photobases could be utilized to drive photochemically the reactions that require either hydroxide ions or other anionic species (such as alkoxyde ions). In order to investigate this possibility, AcrOMe derivative was used as a system that, upon excitation, releases methoxyde (MeO^-) ion. The photogenerated MeO^- ions were successfully utilized in a model Michael addition between dimethylmalonate 1 and nitrostyrene 3 (Scheme 2), in a reaction that involves three individual steps: (i) deprotonation of malonate 1 using the photogenerated MeO^- ions; (ii) nucleophilic attack of the enolate 2 to the electron-deficient $\text{C}=\text{C}$ bond of nitrostyrene 3; (iii) protonation of the intermediate 4 to give the final product 5.



Scheme 2. Model Photo-Michael addition between nitrostyrene and dimethylmalonate using a light-triggered base AcrOMe.

While Michael additions often requires only catalytic amounts of the base, the model reaction presented in Scheme 2 requires stoichiometric amounts of the MeO^- ion. Experiments that

1
2
3 utilized a lower number of MeO^- equivalents yielded less product, indicating that the turnover
4 frequency (TOF) of the catalytic cycle is not sufficiently high to compete with other unwanted
5 chemical reactions. The likely reason for low catalytic TOF is the low basicity of the
6 intermediate 4, which prevents it from abstracting a proton from malonate 1 (a step that is
7 needed to close the catalytic cycle): the acidity of compound 5 is expected to be similar to that of
8 nitromethane ($\text{pK}_a=10$),⁷⁰ while the acidity of malonate 1 is $\text{pK}_a=13$.⁷¹ However, this model
9 reaction is expected to serve as a proof-of-principle study for development of future reactions in
10 which the pK_a values of relevant reactants are tailored towards catalysis.
11
12
13
14
15
16
17
18
19
20
21

22 When the reaction mixture containing AcrOMe was photo-irradiated, the product yield was
23 found to be 60%. The reaction mixture was heated to 65 °C, since the addition step II does not
24 occur at room temperature. When the same reaction was performed in the absence of light, the
25 product yield was only 38%, indicating that the AcrOMe performance can be significantly
26 improved using photochemical methods. However, the results show that reaction occurs even in
27 the absence of irradiation, possibly due to the thermal heterolysis of AcrOMe bond. This finding
28 is consistent with the fact that the Gibbs free energy for AcrOMe heterolysis is expected to be
29 $\Delta G_{\text{OMe}} \sim -6.4$ kcal/mol (similar to that of AcrOH, Table 1). At the reaction temperature of 65 °C, at
30 least 1% of the AcrOMe is expected to thermally dissociate into Acr^+ and MeO^- ions, which can
31 drive the ‘dark’ Michael addition. The contrast in the reaction yields between the dark and
32 photochemical Michael reactions can likely be increased if the choice of reactants was made to
33 perform the reaction at room temperature.
34
35
36
37
38
39
40
41
42
43
44
45
46
47
48
49

50 CONCLUSIONS

51
52 The excited-state OH^- transfer has been studied to a lesser degree relative to the corresponding
53 PT reactions. This manuscript aims to bridge the gap by investigating the parameters that affect
54
55
56
57
58
59
60

1
2
3 the kinetics of the OH⁻ release from model acridinol photobases. The thermodynamic driving
4 force for the reaction was tuned using a series of acridinol derivatives with varying substituents
5 on the phenyl ring, while the reaction rates were determined using time-resolved laser
6 spectroscopy. The experimentally obtained rate constants and Gibbs free energies were fit using
7 the Marcus model for group transfer reactions. The fitted data provided an intrinsic
8 reorganization energy, which matches surprisingly well with the solvent reorganization energies
9 calculated using a simple dielectric continuum model. The results of this study indicate that the
10 solvent reorganization plays a major role in the kinetics of the excited-state OH⁻ release and can
11 be efficiently modeled using the Marcus model. These results are in contrast to our previous
12 study involving a xanthenol photobase in acetonitrile/water mixtures,³⁶ where the experimentally
13 obtained reorganization energy was significantly higher than the solvent reorganization energy
14 predicted by the dielectric continuum model. The observed discrepancy could be due to strong
15 specific solvent-solute interactions present in aqueous environment.
16
17
18
19
20
21
22
23
24
25
26
27
28
29
30
31
32
33

34 This manuscript also evaluates the utilization of acridinol photobases in driving useful chemical
35 reactions. Specifically, the Michael addition between dimethylmalonate and nitrostyrene was
36 successfully performed using MeO⁻ base that was photochemically generated from the
37 corresponding AcrOMe derivatives. While the reported reaction also occurred thermally (with a
38 lower yield), the results indicate that the photo-Michael addition reported here can be further
39 optimized and developed into a useful photochemical tool for applications where spatial-
40 temporal control is needed.
41
42
43
44
45
46
47
48
49
50
51
52

53 AUTHOR INFORMATION

54
55 *Corresponding author e-mails: kglusac@bgsu.edu (K. D. G.)
56
57
58
59
60

1
2
3
4
5
6
7
8
9
10
11
12
13
14
15
16
17
18
19
20
21
22
23
24
25
26
27
28
29
30
31
32
33
34
35
36
37
38
39
40
41
42
43
44
45
46
47
48
49
50
51
52
53
54
55
56
57
58
59
60

¹Current address: Department of Petroleum Engineering, University of Wyoming, Laramie, Wyoming 82071, United States

ACKNOWLEDGEMENTS

KDG thanks National Science Foundation (1055397) and Petroleum Research Fund (54436-ND4) for the financial support.

REFERENCES

1. Arnaut, L. G.; Formosinho, S. J., Excited-State Proton Transfer Reactions I. Fundamentals and Intermolecular Reactions. *J. Photochem. Photobiol. A* **1993**, *75* (1), 1-20.
2. Tolbert, L. M.; Solntsev, K. M., Excited-State Proton Transfer: From Constrained Systems to “Super” Photoacids to Superfast Proton Transfer. *Acc. Chem. Res.* **2002**, *35* (1), 19-27.
3. Agmon, N., Elementary Steps in Excited-State Proton Transfer. *J. Phys. Chem. A* **2005**, *109* (1), 13-35.
4. Huppert, D.; Kolodney, E.; Gutman, M.; Nachliel, E., Effect of Water Activity on the Rate of Proton Dissociation. *J. Am. Chem. Soc.* **1982**, *104* (25), 6949-6953.
5. Agmon, N.; Huppert, D.; Masad, A.; Pines, E., Excited-State Proton Transfer to Methanol-Water Mixtures. *J. Phys. Chem.* **1991**, *95* (25), 10407-10413.
6. Rini, M.; Magnes, B.-Z.; Pines, E.; Nibbering, E. T., Real-Time Observation of Bimodal Proton Transfer in Acid-Base Pairs in Water. *Science* **2003**, *301* (5631), 349-352.

- 1
2
3 7. Mohammed, O. F.; Pines, D.; Dreyer, J.; Pines, E.; Nibbering, E. T., Sequential Proton
4 Transfer Through Water Bridges in Acid-Base Reactions. *Science* **2005**, *310* (5745), 83-86.
5
6
7
8
9 8. Siwick, B. J.; Bakker, H. J., On the Role of Water in Intermolecular Proton-Transfer
10 Reactions. *J. Am. Chem. Soc.* **2007**, *129* (44), 13412-13420.
11
12
13
14 9. Liu, W.; Han, F.; Smith, C.; Fang, C., Ultrafast Conformational Dynamics of Pyranine
15 during Excited State Proton Transfer in Aqueous Solution Revealed by Femtosecond Stimulated
16 Raman Spectroscopy. *J. Phys. Chem. B* **2012**, *116* (35), 10535-10550.
17
18
19
20
21
22 10. Adamczyk, K.; Prémont-Schwarz, M.; Pines, D.; Pines, E.; Nibbering, E. T., Real-Time
23 Observation of Carbonic Acid Formation in Aqueous Solution. *Science* **2009**, *326* (5960), 1690-
24 1694.
25
26
27
28
29
30 11. Das, R.; Mitra, S.; Nath, D.; Mukherjee, S., Excited State Proton Transfer Reaction as a
31 Probe for the Microenvironment of a Binding Site of Bovine Serum Albumin: Effect of Urea. *J.*
32 *Phys. Chem.* **1996**, *100* (34), 14514-14519.
33
34
35
36
37
38 12. Nachliel, E.; Pollak, N.; Huppert, D.; Gutman, M., Time-Resolved Study of the Inner
39 Space of Lactose Permease. *Biophys. J.* **2001**, *80* (3), 1498-1506.
40
41
42
43 13. Cohen, B.; Martin Álvarez, C.; Alarcos Carmona, N.; Organero, J. A.; Douhal, A.,
44 Proton-Transfer Reaction Dynamics within the Human Serum Albumin Protein. *J. Phys. Chem.*
45 *B* **2011**, *115* (23), 7637-7647.
46
47
48
49
50
51 14. Shvadchak, V. V.; Falomir-Lockhart, L. J.; Yushchenko, D. A.; Jovin, T. M., Specificity
52 and Kinetics of α -Synuclein Binding to Model Membranes Determined with Fluorescent Excited
53
54
55
56
57
58
59
60

1
2
3 State Intramolecular Proton Transfer (ESIPT) Probe. *J. Biol. Chem.* **2011**, *286* (15), 13023-
4
5
6 13032.

7
8
9 15. Chowdhury, R.; Saha, A.; Mandal, A. K.; Jana, B.; Ghosh, S.; Bhattacharyya, K., Excited
10
11 State Proton Transfer in the Lysosome of Live Lung Cells: Normal and Cancer Cells. *J. Phys.*
12
13 *Chem. B* **2015**, *119* (6), 2149-2156.

14
15
16
17 16. van Thor, J. J., Photoreactions and Dynamics of the Green Fluorescent Protein. *Chem.*
18
19 *Soc. Rev.* **2009**, *38* (10), 2935-2950.

20
21
22
23 17. Chattoraj, M.; King, B. A.; Bublitz, G. U.; Boxer, S. G., Ultra-Fast Excited State
24
25 Dynamics in Green Fluorescent Protein: Multiple States and Proton Transfer. *Proc. Natl. Acad.*
26
27 *Sci.* **1996**, *93* (16), 8362-8367.

28
29
30
31 18. Gepshtein, R.; Leiderman, P.; Huppert, D.; Project, E.; Nachliel, E.; Gutman, M., Proton
32
33 Antenna Effect of the γ -Cyclodextrin Outer Surface, Measured by Excited State Proton Transfer.
34
35 *J. Phys. Chem. B* **2006**, *110* (51), 26354-26364.

36
37
38
39 19. Cohen, B.; Huppert, D.; Solntsev, K. M.; Tsfadia, Y.; Nachliel, E.; Gutman, M., Excited
40
41 State Proton Transfer in Reverse Micelles. *J. Am. Chem. Soc.* **2002**, *124* (25), 7539-7547.

42
43
44
45 20. Spry, D.; Goun, A.; Glusac, K.; Moilanen, D. E.; Fayer, M., Proton Transport and the
46
47 Water Environment in Nafion Fuel Cell Membranes and AOT Reverse Micelles. *J. Am. Chem.*
48
49 *Soc.* **2007**, *129* (26), 8122-8130.

50
51
52
53 21. Abbruzzetti, S.; Viappiani, C.; Small, J. R.; Libertini, L. J.; Small, E. W., Kinetics of
54
55 Histidine Deligation from the Heme in GuHCl-Unfolded Fe (III) Cytochrome C Studied by a
56
57 Laser-Induced pH-Jump Technique. *J. Am. Chem. Soc.* **2001**, *123* (27), 6649-6653.
58
59
60

- 1
2
3 22. Kohse, S.; Neubauer, A.; Pazidis, A.; Lochbrunner, S.; Kragl, U., Photoswitching of
4 enzyme activity by laser-induced pH-jump. *Journal of the American Chemical Society* **2013**, *135*
5
6 (25), 9407-9411.
7
8
9
10
11 23. Wan, P.; Yates, K.; Boyd, M. K., Adiabatic Photodehydroxylation of 9-Phenylxanthen-9-
12 ol. Observation of Carbocation Fluorescence in Neutral Aqueous Solution. *J. Org. Chem.* **1985**,
13
14 *50* (16), 2881-2886.
15
16
17
18
19 24. Wan, P.; Krogh, E., Contrasting Photosolvolytic Reactivities of 9-Fluorenone vs. 5-
20 Suberenol Derivatives. Enhanced Rate of Formation of Cyclically Conjugated 4π Carbocations
21 in the Excited State. *J. Am. Chem. Soc.* **1989**, *111* (13), 4887-4895.
22
23
24
25
26
27 25. Wan, P.; Shukla, D., Utility of Acid-Base Behavior of Excited States of Organic
28 Molecules. *Chem. Rev.* **1993**, *93* (1), 571-584.
29
30
31
32
33 26. Das, P., Transient Carbocations and Carbanions Generated by Laser Flash Photolysis and
34 Pulse Radiolysis. *Chem. Rev.* **1993**, *93* (1), 119-144.
35
36
37
38 27. Pischel, U.; Abraham, W.; Schnabel, W.; Müller, U., The Photogeneration of
39 Aryltropylium Ions: A Potential Photo-Switch for Supramolecular Assemblies Based on Donor-
40 Acceptor Interaction. *Chem. Commun.* **1997**, (15), 1383-1384.
41
42
43
44
45
46 28. Abraham, W.; Buck, K.; Orda-Zgadzaj, M.; Schmidt-Schäffer, S.; Grummt, U.-W., Novel
47 Photoswitchable Rotaxanes. *Chem. Commun.* **2007**, (29), 3094-3096.
48
49
50
51
52 29. Raskosova, A.; Stößer, R.; Abraham, W., Molecular Photoswitches Based on Spiro-
53 Acridans. *Chem. Commun.* **2013**, *49* (38), 3964-3966.
54
55
56
57
58
59
60

- 1
2
3
4
5
6
7
8
9
10
11
12
13
14
15
16
17
18
19
20
21
22
23
24
25
26
27
28
29
30
31
32
33
34
35
36
37
38
39
40
41
42
43
44
45
46
47
48
49
50
51
52
53
54
55
56
57
58
59
60
30. Agmon, N., Mechanism of Hydroxide Mobility. *Chem. Phys. Lett.* **2000**, *319* (3), 247-252.
31. Marx, D.; Chandra, A.; Tuckerman, M. E., Aqueous Basic Solutions: Hydroxide Solvation, Structural Diffusion, and Comparison to the Hydrated Proton. *Chem. Rev.* **2010**, *110* (4), 2174-2216.
32. WooáLee, S.; SungáYoon, D., Nanomechanical Actuation Driven by Light-Induced DNA Fuel. *Chem. Commun.* **2012**, *48* (7), 955-957.
33. Liu, H.; Xu, Y.; Li, F.; Yang, Y.; Wang, W.; Song, Y.; Liu, D., Light□Driven Conformational Switch of i□Motif DNA. *Angew. Chem. Int. Ed.* **2007**, *46* (14), 2515-2517.
34. Carvalho, C. P.; Uzunova, V. D.; Da Silva, J. P.; Nau, W. M.; Pischel, U., A Photoinduced pH-Jump Applied to Drug Release from Cucurbit[7]uril. *Chem. Commun.* **2011**, *47* (31), 8793-8795.
35. Zhou, D.; Khatmullin, R.; Walpita, J.; Miller, N. A.; Luk, H. L.; Vyas, S.; Hadad, C. M.; Glusac, K. D., Mechanistic Study of the Photochemical Hydroxide Ion Release from 9-Hydroxy-10-methyl-9-phenyl-9, 10-dihydroacridine. *J. Am. Chem. Soc.* **2012**, *134* (28), 11301-11303.
36. Xie, Y.; Luk, H. L.; Yang, X.; Glusac, K. D., Excited-State Hydroxide Ion Transfer from a Model Xanthenol Photobase. *J. Phys. Chem. B* **2015**, *119*, 2498-2506.
37. Prémont-Schwarz, M.; Barak, T.; Pines, D.; Nibbering, E. T.; Pines, E., Ultrafast Excited-State Proton-Transfer Reaction of 1-Naphthol-3, 6-Disulfonate and Several 5-Substituted 1-Naphthol Derivatives. *J. Phys. Chem. B* **2013**, *117* (16), 4594-4603.

1
2
3 38. Keitz, B. K.; Yu, C. J.; Long, J. R.; Ameloot, R., Lithographic Deposition of Patterned
4 Metal–Organic Framework Coatings Using a Photobase Generator. *Angew. Chem. Int. Ed.* **2014**,
5
6 53 (22), 5561-5565.
7

8
9
10
11 39. Cameron, J. F.; Willson, C. G.; Fréchet, J. M., Photogeneration of Amines from α -Keto
12 Carbamates: Photochemical Studies. *J. Am. Chem. Soc.* **1996**, 118 (51), 12925-12937.
13

14
15
16
17 40. Sun, X.; Gao, J. P.; Wang, Z. Y., Bicyclic Guanidinium Tetraphenylborate: A Photobase
18 Generator and a Photocatalyst for Living Anionic Ring-Opening Polymerization and Cross-
19 Linking of Polymeric Materials Containing Ester and Hydroxy Groups. *J. Am. Chem. Soc.* **2008**,
20 130 (26), 8130-8131.
21

22
23
24
25 41. Peters, M. V.; Stoll, R. S.; Kühn, A.; Hecht, S., Photoswitching of Basicity. *Angew.*
26 *Chem. Int. Ed.* **2008**, 47 (32), 5968-5972.
27

28
29
30
31 42. He, J.; Kimani, F. W.; Jewett, J. C., A Photobasic Functional Group. *J. Am. Chem. Soc.*
32 **2015**, 137 (31), 9764-9767.
33

34
35
36
37 43. Gleu, K.; Schubert, A., Die Kondensation der Phosphoroxychlorid- \square Acridone mit
38 Dimethylanilin. *Berichte der deutschen chemischen Gesellschaft (A and B Series)* **1940**, 73 (7),
39 757-761.
40

41
42
43
44 44. Jones, G.; Farahat, M. S.; Greenfield, S. R.; Gosztola, D. J.; Wasielewski, M. R.,
45 Ultrafast Photoinduced Charge-Shift Reactions in Electron Donor-Acceptor 9-Arylacridinium
46 ions. *Chem. Phys. Lett.* **1994**, 229 (1), 40-46.
47

48
49
50
51 45. Deno, N.; Jaruzelski, J.; Schriesheim, A., Carbonium Ions. I. An Acidity Function (C0)
52 Derived from Arylcarbonium Ion Equilibria¹. *J. Am. Chem. Soc.* **1955**, 77 (11), 3044-3051.
53
54
55
56
57
58
59
60

1
2
3
4
5
6
7
8
9
10
11
12
13
14
15
16
17
18
19
20
21
22
23
24
25
26
27
28
29
30
31
32
33
34
35
36
37
38
39
40
41
42
43
44
45
46
47
48
49
50
51
52
53
54
55
56
57
58
59
60

46. Ito, S.; Morita, N.; Asao, T., Syntheses of Azulene Analogues of Triphenylmethyl Cation: Extremely Stable Hydrocarbon Carbocations and the First Example of a One-Ring Flip as the Threshold Rotation Mechanism for Molecular Propellers. *Bull. Chem. Soc. Jpn.* **1995**, *68* (5), 1409-1436.

47. Zhang, X.-M.; Bruno, J. W.; Enyinnaya, E., Hydride Affinities of Arylcarbenium Ions and Iminium Ions in Dimethyl Sulfoxide and Acetonitrile. *J. Org. Chem.* **1998**, *63* (14), 4671-4678.

48. Pines, D.; Pines, E., Solvent Assisted Photoacidity. Wiley-VCH: Weinheim, Germany: 2007; Vol. 1, p 377.

49. Hansch, C.; Leo, A.; Taft, R., A Survey of Hammett Substituent Constants and Resonance and Field Parameters. *Chem. Rev.* **1991**, *91* (2), 165-195.

50. Pines, E.; Fleming, G. R., Proton Transfer in Mixed Water-Organic Solvent Solutions: Correlation between Rate, Equilibrium Constant, and the Proton Free Energy of Transfer. *J. Phys. Chem.* **1991**, *95* (25), 10448-10457.

51. Tolbert, L. M.; Harvey, L. C.; Lum, R. C., Excited-State Proton Transfer from Hydroxyalkylnaphthols. *J. Phys. Chem.* **1993**, *97* (50), 13335-13340.

52. Minto, R. E.; Das, P. K., Laser Flash Photolysis Study of Photodehydroxylation Phenomena of 9-Phenylxanthen-9-ol and Photobehavior of Related Intermediates. Enhanced Electrophilicity of 9-Phenylxanthenium Cation Singlet. *J. Am. Chem. Soc.* **1989**, *111* (24), 8858-8866.

53. Haynes, W. M., *CRC handbook of chemistry and physics*. CRC press: 2014.

1
2
3 54. Dalton, J. C.; Montgomery, F. C., Solvent Effects on Thioxanthone Fluorescence. *J. Am.*
4
5
6 *Chem. Soc.* **1974**, *96* (19), 6230-6232.

7
8
9 55. Cavaleri, J. J.; Prater, K.; Bowman, R. M., An Investigation of the Solvent Dependence
10
11 on the Ultrafast Intersystem Crossing Kinetics of Xanthone. *Chem. Phys. Lett.* **1996**, *259* (5),
12
13 495-502.

14
15
16 56. Marcus, R. A., On the Theory of Oxidation-Reduction Reactions Involving Electron
17
18 Transfer. I. *J. Chem. Phys.* **1956**, *24* (5), 966-978.

19
20
21 57. Marcus, R., On the Theory of Oxidation-Reduction Reactions Involving Electron
22
23 Transfer. II. Applications to Data on the Rates of Isotopic Exchange Reactions. *J. Chem. Phys.*
24
25 **1957**, *26* (4), 867-871.

26
27
28 58. Marcus, R., Chemical and Electrochemical Electron-Transfer Theory. *Annu. Rev. Phys.*
29
30
31 *Chem.* **1964**, *15* (1), 155-196.

32
33
34 59. Miller, J.; Calcaterra, L.; Closs, G., Intramolecular Long-Distance Electron Transfer in
35
36 Radical Anions. The Effects of Free Energy and Solvent on the Reaction Rates. *J. Am. Chem.*
37
38
39 *Soc.* **1984**, *106* (10), 3047-3049.

40
41
42 60. Johnston, H. S.; Parr, C., Activation Energies from Bond Energies. I. Hydrogen Transfer
43
44
45 Reactions. *J. Am. Chem. Soc.* **1963**, *85* (17), 2544-2551.

46
47
48 61. Chandra, A.; Rao, V. S., An Examination of the BEBO Model with the Results of Ab
49
50
51 Initio Calculations of a Reaction Series. *Chem. Phys.* **1994**, *187* (3), 297-303.

52
53
54 62. Marcus, R. A., Theoretical Relations among Rate Constants, Barriers, and Brønsted
55
56
57 Slopes of Chemical Reactions. *J. Phys. Chem.* **1968**, *72* (3), 891-899.
58
59
60

1
2
3 63. Marcus, R. A., On the Theory of Electron-Transfer Reactions. VI. Unified Treatment for
4 Homogeneous and Electrode Reactions. *J. Chem. Phys.* **1965**, *43* (2), 679-701.
5
6

7
8
9 64. Oevering, H.; Paddon-Row, M. N.; Heppener, M.; Oliver, A. M.; Cotsaris, E.;
10 Verhoeven, J. W.; Hush, N. S., Long-Range Photoinduced Through-Bond Electron Transfer and
11 Radiative Recombination via Rigid Nonconjugated Bridges: Distance and Solvent Dependence.
12 *J. Am. Chem. Soc.* **1987**, *109* (11), 3258-3269.
13
14
15

16
17
18 65. Hupp, J. T.; Weaver, M. J., Noncontinuum Solvent Effects upon the Intrinsic Free-
19 Energy Barrier for Electron-Transfer Reactions. *J. Phys. Chem.* **1985**, *89* (9), 1601-1608.
20
21
22

23
24
25 66. Chen, P.; Meyer, T. J., Medium Effects on Charge Transfer in Metal Complexes. *Chem.*
26 *Rev.* **1998**, *98* (4), 1439-1478.
27
28

29
30 67. Nelsen, S. F.; Trieber, D. A.; Ismagilov, R. F.; Teki, Y., Solvent Effects on Charge
31 Transfer Bands of Nitrogen-Centered Intervalence Compounds. *J. Am. Chem. Soc.* **2001**, *123*
32 (24), 5684-5694.
33
34
35

36
37
38 68. Xi, W.; Peng, H.; Aguirre-Soto, A.; Kloxin, C. J.; Stansbury, J. W.; Bowman, C. N.,
39 Spatial and Temporal Control of Thiol-Michael Addition via Photocaged Superbase in
40 Photopatterning and Two-Stage Polymer Networks Formation. *Macromolecules* **2014**, *47* (18),
41 6159-6165.
42
43
44

45
46
47 69. Zhang, X.; Xi, W.; Wang, C.; Podgórski, M.; Bowman, C. N., Visible-Light-Initiated
48 Thiol-Michael Addition Polymerizations with Coumarin-Based Photobase Generators: Another
49 Photoclick Reaction Strategy. *ACS Macro Lett.* **2016**, *5* (2), 229-233.
50
51
52

53
54
55
56 70. Bell, R. P., *The Proton in Chemistry*. Springer Science & Business Media: 2013.
57
58
59
60

1
2
3 71. March, J., *Advanced Organic Chemistry: Reactions, Mechanisms, and Structure*. John
4
5
6 Wiley & Sons: 1992.

7
8
9
10
11
12 TOC Graphic

